RSC Advances

ROYAL SOCIETY OF CHEMISTRY

www.rsc.org/advances

A study on the effect of K_2ZrF_6 as an additive on the microstructure and hydrogen storage properties of MgH_2

F.A. Halim Yap, N. S. Mustafa, M. Ismail*

School of Ocean Engineering, Universiti Malaysia Terengganu, 21030 Kuala Terengganu, Malaysia

*Corresponding author. Tel: +609-6683487; Fax: +609-6683991

E-mail address: mohammadismail@umt.edu.my

Abstract

In this work, the hydrogenation properties of MgH_2-doped K_2ZrF_6 with X wt.% (X=5, 10, 15 and 20) have been investigated for the first time. Analysis indicated that MgH_2 doped with 10 wt.% K_2ZrF_6 is the best composite in the improvement of the hydrogen storage properties of MgH_2. The results showed that the onset desorption temperature after the addition of 10 wt.% K_2ZrF_6 was 250 ºC, which experienced the reduction of 100 °C and 200 °C from 350 ºC and 450 ºC for as-milled and as-received MgH_2 respectively. The re/dehydrogenation kinetics had also improved significantly compared to the un-doped MgH_2. The results of the Arrhenius plot exhibited that the activation energy for the hydrogen desorption of MgH_2 was reduced from 164 kJ/mol to 80 kJ/mol after the addition of 10 wt% K_2ZrF_6. Meanwhile, the X-ray diffraction spectra displayed the formation of a new phase of KH and ZrH_2 through the doping of K_2ZrF_6 with MgH_2 after the dehydrogenation and rehydrogenation processes. These two compounds are believed to act as the active species and play a catalytic role in improving the hydrogen storage properties. It is therefore concluded that this newly developed catalytic doping system works well in improving the hydrogen sorption properties of MgH_2.

1. Introduction

Even though hydrogen is an ideal energy carrier, there are still extensive technological challenges that delay its uses as a fuel. Hydrogen can be used as a fuel in PEMFC (proton exchange membrane fuel cell), which is a very promising power source for electric vehicle (EV).[1] According to the U.S. DOE's 2010 target, large volumetric (>62 kgm^{-3}) and gravimetric (>6.5 wt.%) densities are strictly needed for an on-board hydrogen storage in fuel cell vehicles. To realize that, a high-performance hydrogen storage system is desired in order to accomplish the DOE's target. High-pressure and cryogenic hydrogen storage systems are impractical for vehicular applications due to safety anxieties and volumetric constraints. In current years, attention has been focused on solid hydrogen storage materials due to the significant advantages related to safety, energy efficiency and effective cost.[2] To date, many types of solid-state hydrogen storage materials have been explored, such as metal hydrides,[3-6] complex hydrides,[7-13] carbon materials,[14, 15] and metal-organics frameworks (MOFs).[16, 17] Among all of these materials, metal hydrides have attracted intensive research interest because of their high hydrogen storage capacities and moderate working temperatures. Among the various metal hydrides, MgH_2 is highly recommended due to its high hydrogen capacity with a theoretical value of 7.6 wt.%, high reversibility, low cost[18-20] and reserves in the earth's crust.[21] Therefore, MgH_2 is viewed as one of the most promising hydrogen storage materials. Unfortunately, the practical application of MgH_2 is greatly delayed by the slow kinetics and high operation temperature.[22] Its working temperature is above 300 ºC and the de/re-hydrogenation kinetics is slow, which limits its practical application for on-board hydrogen storage. To overcome these problems, much effort has been done in this past decade to improve its hydrogen storage properties, such as combining with other materials (destabilization of the system),[23-30] improving the surface and kinetics by ball milling,[31] and doping with catalysts.[32-36] Among them, the introduction of catalysts or additives into MgH_2

by ball milling method has shown a significant effect on the hydrogen storage properties of MgH_2.

Another promising additive for MgH_2 is K_2ZrF_6. It is believed that upon heating, K_2ZrF_6 and MgH_2 will react by an in-situ reaction to form active species that would enhance the hydrogen sorption properties of MgH_2. Xiao et al.[37] demonstrated that the superior effects of KH on improving the dehydrogenation properties of $NaAlH_4$. It has also been confirmed that ZrH_2 could provide favourable effects on enhancing the dehydrogenation properties of MgH_2.[38] Therefore, it is reasonable to believe that K_2ZrF_6 shows a great potential as an additive to advance the hydrogen storage properties of MgH_2 through combining together these in-situ metal hydride positive factors.

In this work, K_2ZrF_6 was introduced to examine the improvement of the hydrogen storage performance of the MgH_2 obtained by ball milling. To the best of the author's knowledge, no studies have reported the effect of K_2ZrF_6 on the microstructure and hydrogen storage properties of MgH_2. The hydrogen storage properties and reaction mechanisms of MgH_2 and K_2ZrF_6 were investigated in experiments using a Sievert-type pressure-composition-temperature (PCT) apparatus, scanning electron microscope (SEM) and X-ray diffraction (XRD). The possible catalysis mechanism supported by the results of the experiment was then discussed.

2. Experimental details

Pure MgH_2 (hydrogen storage grade with 98% purity) and K_2ZrF_6 (97% purity) were purchased from Sigma Aldrich and were used as received without further purification. Approximately 200 mg of MgH_2 and doped with 20 mg of K_2ZrF_6 was loaded into a sealed stainless steel vial together with four hardened stainless steel balls in an argon atmosphere MBraun Unilab glove box. For simplicity, the mixture of MgH_2 with 10 wt.% of K_2ZrF_6 will

be referred to as MgH_2-10 wt.% K_2ZrF_6 sample. The sample was then milled in a planetary ball mill (NQM-0.4) for 1 h, first by milling for 0.25 h, rest for 2 min, and then the milling was repeated for another 2 cycles in a different direction at the rate of 400 rpm. The as-received MgH_2 was also prepared under the same conditions for comparison purposes. The de/rehydrogenation experiments were performed in a Sievert-type pressure-composition-temperature (PCT) apparatus (Advanced Materials Corporation). The composite was loaded into a sample vessel in the glove box. For the temperature-programmed-desorption (TPD) experiment, all the composites were heated in a vacuum chamber, and the amount of desorbed hydrogen was measured to determine the lowest decomposition temperature. The heating rate for the TPD experiment was 5 ºCmin^{-1}, and the samples were heated from room temperature to 450 ºC. The re/dehydrogenation kinetics measurements were performed at the desired temperature with the initial hydrogen pressures of 33.00 atm and 1.00 atm respectively.

XRD analysis was performed using a Rigaku MiniFlex X-ray diffractometer, with Cu Ka radiation scans were carried out over the diffraction angles from 20 ° to 80 ° with a speed of 2 °min^{-1}. Prior to the measurement, a small amount of sample was placed uniformly on the sample holder, which was wrapped with plastic wrap to avoid oxidation. Meanwhile, the surface morphology of the composite was observed using scanning electron microscope (SEM; JEOL JSM-6360LA) by setting the samples on carbon tape and then the samples were coated with gold spray under vacuum.

3. Results and discussion

3.1 Dehydrogenation Temperature

Figure 1 shows the TPD performances for the dehydrogenation of as-received MgH_2, as-milled MgH_2 and the MgH_2 doped with 5 wt.%, 10 wt.%, 15 wt.% and 20 wt.% K_2ZrF_6.

From the TPD patterns, it is obvious that by doping with a 5 wt.% to 20 wt.% of K_2ZrF_6 to MgH_2 was resulted in a drop of the onset desorption temperature rather than un-doped MgH_2. The as-received MgH_2 started to dehydrogenate H_2 at the temperature 450 ℃ and the total dehydrogenation capacity is 7.5 wt.% H_2. The onset desorption temperature of MgH_2 after milling was slightly drop to about 350 ℃, showing that the process of milling was also affected the onset desorption temperature [31]. After milling, the curve shows that there was no reduction in the hydrogen desorption capacity of MgH_2. The addition of K_2ZrF_6 greatly improved the onset desorption temperature for MgH_2. For the MgH_2 doped with 5 wt.% K_2ZrF_6 started to decompose at about 260 ℃, with a total dehydrogenation capacity of 6.6 wt.% H_2. The 10 wt.% doped sample, the dehydrogenation was at 250 ℃, which was a decrease in the desorption onset of about 100 ℃ from 350 ℃ for as-milled MgH_2, with a total dehydrogenation capacity of 6.6 wt.% H_2, which was the same as the hydrogen desorption capacity of the 5 wt.% doped sample. A further increase of the doping amounts to 15 wt.% and 20 wt.% reduced the desorption onset temperatures to about 280 ℃ and 290 ℃, but the amount of hydrogen released slightly dropped to about 5.6 wt.% and 5.3 wt.% H_2, respectively. This phenomena may due to the excessive catalytic effect brought about by the relatively high level of the added K_2ZrF_6 and this result almost the same with our previous paper [19].

3.2 Re/dehydrogenation Kinetics

Figure 2 depicts the hydrogen absorption rate of MgH_2 after ball milling for an hour and MgH_2 doped with K_2ZrF_6 samples also by an hour milling at 300 ℃ under 33.0 atm. The results were compared and it was shown that MgH_2 with ball milling after an hour can absorb about 3.3 wt.% of H_2 in 5 min and approximately 4.0 wt.% of H_2 in 60 min. On the other hand, after adding 10 wt.% K_2ZrF_6 into MgH_2, it was shown that a slight improvement has been attained. About 3.5 wt.% of H_2 can be absorbed in 5 min and approximately 4.1 wt.% of

H_2 could be absorbed in 60 min. Meanwhile for the 5 wt.%, 15 wt.% and 20 wt.% K_2ZrF_6-doped MgH_2, the hydrogen absorbs as much as 3.2 wt.%, 3.3 wt.% and 3.0 wt.% H_2 within 5 min. Figure 3 displays that the samples MgH_2 doped with 5 wt.%, 10 wt.%, 15 wt.% and 20 wt.% K_2ZrF_6 release hydrogen about 3.7 wt.%, 4.1 wt.%, 4.0 wt.% and 3.6 wt.% at 300 °C in 60 min, respectively, whereas the un-doped MgH_2 sample desorbed just 0.3 wt.% hydrogen in the same period of time. The doped composites displayed an enhancement in terms of desorption kinetics. The result of the desorption onset temperature and isothermal re/dehydrogenation kinetics indicates that the sample of 10 wt.% K_2ZrF_6 shows the best performance to improve the hydrogen storage properties of MgH_2 and thus can be considered as the best samples for MgH_2 doped K_2ZrF_6. Therefore, the addition of 10 wt.% K_2ZrF_6 doped with MgH_2 is chosen for further analysis.

Furthermore, to further analyse the hydrogen desorption kinetics of the MgH_2-10 wt.% K_2ZrF_6 sample, isothermal dehydrogenation measurements were performed at different temperature. Figure 4 compares the isothermal dehydrogenation kinetics between the as-milled MgH_2 and MgH_2-10 wt.% K_2ZrF_6 samples at 300 ºC, 320 ºC and 350 °C. The dehydrogenation kinetics test was carried out after the rehydrogenation kinetics process under 33.0 atm of H_2 at 300 °C, 320 °C and 350 °C. The result was as expected as the dehydrogenation rate for the as-milled MgH_2 was lower than the doped MgH_2 at 350 °C (Figure 4(c, f)). After the addition of K_2ZrF_6, the desorption kinetics increased significantly as the 10 wt.% K_2ZrF_6-doped MgH_2 could release 4.5 wt.% of H_2 within 10 min at 350 °C. Under the same conditions, it was shown that the amount of hydrogen released from the as-milled MgH_2 were less than 0.5 wt.% and only 2 wt.% even after 20 min. Further investigation on the 10 wt.% K_2ZrF_6-doped MgH_2 at 300 °C and 320 °C showed a similar result (Figure 4((a, d), (b, e))), where doped MgH_2 revealed better desorption kinetics than the un-doped MgH_2. This improvement is due to the energy barrier, where the activation

energy for hydrogen to be released from MgH_2 is reduced by the addition of K_2ZrF_6. The activation energy can be calculated by using the Arrhenius equation as follows:

$$k = k_0 \exp(-E_A/RT) \quad (1)$$

Where k is the rate of hydrogenation, k_0 is a temperature independent coefficient, E_A is the apparent activation energy for hydride decomposition, R is the gas constant and T is the absolute temperature. By plotting the graph of ln(k) vs. 1/T as indicated in Figure 5, the apparent activation energy, E_A for H_2 to be released from the as-milled and K_2ZrF_6-doped MgH_2 was revealed. From the calculation, the activation energy for the as-milled MgH_2 and K_2ZrF_6-doped MgH_2 shown was 80 kJ/mol and 164 kJ/mol respectively. There was an improvement of 84 kJ/mol according to the result. Based on the lowering of the activation energy, the decomposition of the MgH_2 was improved substantially.

The cycling performance of the MgH_2 doped with K_2ZrF_6 composite was further investigated. As shown in Figure 6, temperature of 300 °C were applied in the life cycle study of rehydrogenation kinetics of the MgH_2+10 wt.% K_2ZrF_6 composite. The absorption kinetics continued well, even after the 10th cycle with a capacity of hydrogen about 3.9 wt.%. From the Figure 7, the life cycle desorption kinetics of MgH_2+10 wt.% K_2ZrF_6 at 300 °C shows almost no decrease in hydrogen storage capacity within 60 min even after 10th cycles and being maintained at about 4.1 wt %. The result shows that K_2ZrF_6 is a good additive for the cycle life of MgH_2.

3.3 Scanning electron microscopy

Figure 8 illustrates the grain size of the as-received MgH_2, as-milled MgH_2, and K_2ZrF_6-doped MgH_2. The SEM examination revealed that the grain size before ball milling (Figure 8(a)) was the biggest compared to the as-milled MgH_2 (Figure 8(b)). Meanwhile, as can be seen from Figure 8(c), the grain size of K_2ZrF_6- doped MgH_2 was smaller than the as-milled

MgH_2. The dramatically decreased grain size of doped MgH_2 increased the surface area of contact of MgH_2. As the surface area of contact increases, the rate of reaction for MgH_2 to release and absorb H_2 will increase. Mustafa and Ismail [39] reported that a smaller particle size will improve the hydrogen re/desorption, because it reduces the diffusion length of hydrogen and makes the particles' reactive surfaces larger. Hence, the activation energy and re/desorption will be improved.

3.4 X-ray Diffraction

In order to determine the chemical composition of K_2ZrF_6-doped MgH_2 after milling, XRD scans was performed after the dehydrogenation and after re-hydrogenation processes. Figure 9 depicts the XRD patterns of MgH_2-10 wt% K_2ZrF_6 after 1 h ball milling, after dehydrogenation at 450 ºC and after rehydrogenation at 300 ºC. From the pattern, after 1 h ball milling (Figure 9(a)), only MgH_2 peaks were detected and no K_2ZrF_6-containing phases existed. The absence of the peaks of K_2ZrF_6 might be due to the transformation into amorphous state during the milling or the amount of K_2ZrF_6 might be too little to be detected by the matrix of XRD. After dehydrogenation at 450 °C (Figure 9(b)), distinct peaks of Mg were present, which means the dehydrogenation process was completed. Minor peaks of KH and ZrH_2 were present after the dehydrogenation process as they are the active species of the combination of MgH_2 and K_2ZrF_6 after ball milling or heating process. The spectra of re-hydrogenated K_2ZrF_6-doped MgH_2 (Figure 9(c)) represent major peaks of Mg, where peaks of MgH_2 were less and the active species of KH and ZrH_2 were still present. From the result, it can be determine that MgH_2 is not fully reversible since the peaks of Mg are still present on the rehydrogenation phase.

In order to verify the phase structure of the doped samples in more detail, XRD measurement was performed on the 20 wt.% K_2ZrF_6 added MgH_2 sample. After increasing

the amount of catalyst to 20 wt.%, the peak of KH and ZrH_2 species were increased as shown in Figure 10. Due to the amorphous state, the peak of MgF_2 species could not be observed by XRD pattern. This finding corroborates with the study by Sun et al.[40] that Ag-MgF_2 cermet films consist of mainly amorphous MgF_2 matrix with embedded fcc-Ag nanocrystalline grains. Meanwhile, the absence of Mg peak indicated that by increasing the amount of catalyst to 20 wt.%, MgH_2 can be fully reversible compared to Figure 9. The reaction between MgH_2 and K_2ZrF_6 in the dehydrogenation stage can be represented by the following equation:

$$6MgH_2 + 2K_2ZrF_6 \rightarrow 6MgF_2 + 4KH + 2ZrH_2 + 2H_2 \quad (2)$$

The value for standard Gibbs free energy, ΔG^o_f of MgH_2, MgF_2, KH and ZrH_2 are -35.98, -1071.10, -34.06, and -128.87 kJ/mol [41], respectively. In addition, the standard Gibbs free energy, ΔG^o_f of K_2ZrF_6 is -2456 kJ/mol [42]. Therefore, the total change of $\Delta G°$ will be -1691.26 kJ/mol of MgH_2. This result approves the possibility of reaction (2) from the thermodynamic potentials. The standard-state free energy of reaction, ΔG^o could be calculated as follows:

$$\Delta G^o = \sum \Delta G^o_{f\,products} - \sum \Delta G^o_{f\,reactants} \quad (3)$$

The results of this study prove that the formation of active species of KH and ZrH_2 during the de/rehydrogenation process from the reaction of MgH_2 and K_2ZrF_6 may play an important role to enhance the sorption properties of MgH_2. This discovery verifies the work by Xiao et al.[37] that the addition of KH can effectively improve the dehydrogenation properties of the second step reaction of $NaAlH_4$ system. Besides that, Luo et al.[43] verified that by the addition of catalytic amount (<4 mol %) of catalytic KH significantly increased the hydrogen absorption rate of the desorbed material, and has a less dramatic effect on the kinetics of hydrogen desorption, as also shown by by Wang et al.[44] On the other hand, many findings have exposed that mixing MgH_2 with ZrH_2 improved hydrogenation behaviour.[45, 46]

For example, Kyoi et al.[38] claimed that the mixing of MgH_2 with ZrH_2 to form face centred cubic (FCC) hydrides reduced the hydrogen-desorption temperatures by 170 K lower than that of MgH_2. In addition, among the unbalanced reaction products, ZrH_2 has a very stable phase as reported by Jat et al.[45], as well as excellent stability under irradiation conditions.[46] Therefore, it is sensible to accomplish that this newly developed product of KH and ZrH_2 acts as a real catalyst in enhancing the hydrogen sorption properties of MgH_2 by serving as an active site for nucleation and growth of dehydrogenation products.

Conclusion

In summary, the improvement of the hydrogen desorption properties of MgH_2 have been verified after adding with catalyst K_2ZrF_6. Among the different amounts of K_2ZrF_6, the 10 wt.% of K_2ZrF_6 shows the best performance in improving the hydrogenation properties of MgH_2. The TPD result exhibited that the MgH_2-10 wt% K_2ZrF_6 sample started to release H_2 at about 250 ºC, where the onset desorption temperature was reduced approximately 100 ºC and 200 ºC compared to the as-milled and as-received MgH_2, respectively. The dehydrogenation and rehydrogenation kinetics of the doped MgH_2 also had improved significantly compared to the undoped MgH_2. From the Arrhenius plot, the results showed that the activation energy of MgH_2 after doping 10 wt.% of K_2ZrF_6 was reduced by approximately 84 kJ/mol. Nevertheless, the hydrogen release capacity decreased slightly due to the deadweight of K_2ZrF_6 that contained no hydrogen. In addition, the formation of a new phase of KH and ZrH_2 through the doping of K_2ZrF_6 with MgH_2 during the heating process is believed to act as the active species. Despite all obtained results, it is worthwhile to conclude that the products formed from the addition of K_2ZrF_6 play a catalytic role in improving the hydrogen storage properties of MgH_2.

Acknowledgement

The authors would like to acknowledge Universiti Malaysia Terengganu for providing the facilities to carry out this project. This work was financially supported by the Fundamental Research Grant Scheme (FRGS 59295). F. A. Halim Yap and N.S. Mustafa are thankful to the Ministry of Education Malaysia for the MyBrain15 scholarship.

References

1. J. G. Carton and A. G. Olabi, *Energy*, 2010, 35, 2796-2806.
2. S. Srinivasa Murthy and E. Anil Kumar, *Appl. Therm. Eng.*, 2014.
3. N. S. Mustafa and M. Ismail, *Int. J. Hydrogen Energy*, 2014, 39, 15563-15569.
4. F. Cuevas, D. Korablov and M. Latroche, *Phys. Chem. Chem. Phys.*, 2012, 14, 1200-1211.
5. L. Mooij and B. Dam, *Phys. Chem. Chem. Phys.*, 2013, 15, 11501-11510.
6. X. B. Yu, Y. H. Guo, Z. X. Yang, Z. P. Guo, H. K. Liu and S. X. Dou, *Scripta Mater.*, 2009, 61, 469-472.
7. M. Ismail, Y. Zhao, X. B. Yu and S. X. Dou, *Int. J. Hydrogen Energy*, 2010, 35, 2361-2367.
8. X. B. Yu, Y. H. Guo, D. L. Sun, Z. X. Yang, A. Ranjbar, Z. P. Guo, H. K. Liu and S. X. Dou, *J. Phys. Chem. C*, 2010, 114, 4733-4737.
9. M. Ismail, Y. Zhao, X. B. Yu, A. Ranjbar and S. X. Dou, *Int. J. Hydrogen Energy*, 2011, 36, 3593-3599.
10. X. B. Yu, D. M. Grant and G. S. Walker, *J. Phys. Chem. C*, 2008, 112, 11059-11062.
11. M. Ismail, Y. Zhao, X. B. Yu, I. P. Nevirkovets and S. X. Dou, *Int. J. Hydrogen Energy*, 2011, 36, 8327-8334.

12. Y. Zhang, Q. Tian, J. Zhang, S.-S. Liu and L.-X. Sun, *J. Phys. Chem. C*, 2009, 113, 18424-18430.

13. M. Ismail, *Int. J. Hydrogen Energy*, 2014, 39, 8340-8346.

14. P. Kowalczyk, R. Holyst, M. Terrones and H. Terrones, *Phys. Chem. Chem. Phys.*, 2007, 9, 1786-1792.

15. Y. Zhang, W.-S. Zhang, A.-Q. Wang, S. Li-Xian, M.-Q. Fan, H.-L. Chu, J.-C. Sun and T. Zhang, *Int. J. Hydrogen Energy*, 2007, 32, 3976-3980.

16. M. Hirscher and B. Panella, *J. Alloys Comp.*, 2005, 404-406, 399-401.

17. C.-Y. Wang, C.-S. Tsao, M.-S. Yu, P.-Y. Liao, T.-Y. Chung, H.-C. Wu, M. A. Miller and Y.-R. Tzeng, *J. Alloys Comp.*, 2010, 492, 88-94.

18. A. Ranjbar, Z. P. Guo, X. B. Yu, D. Wexler, A. Calka, C. J. Kim and H. K. Liu, *Materials Chemistry and Physics*, 2009, 114, 168-172.

19. M. Ismail, *Int. J. Hydrogen Energy*, 2014, 39, 2567-2574.

20. M. Y. Song, Y. J. Kwak, H.-S. Shin, S. H. Lee and B.-G. Kim, *Int. J. Hydrogen Energy*, 2013, 38, 1910-1917.

21. S.-S. Liu, L.-X. Sun, J. Zhang, Y. Zhang, F. Xu, Y.-H. Xing, F. Li, J. Zhao, Y. Du, W.-Y. Hu and H.-Q. Deng, *Int. J. Hydrogen Energy*, 2010, 35, 8122-8129.

22. X. B. Yu, Z. X. Yang, H. K. Liu, D. M. Grant and G. S. Walker, *Int. J. Hydrogen Energy*, 2010, 35, 6338-6344.

23. S. Kato, A. Borgschulte, M. Bielmann and A. Zuttel, *Phys. Chem. Chem. Phys.*, 2012, 14, 8360-8368.

24. M. Ismail, Y. Zhao, X. B. Yu, J. F. Mao and S. X. Dou, *Int. J. Hydrogen Energy*, 2011, 36, 9045-9050.

25. Y. Jia, C. Sun, L. Cheng, M. Abdul Wahab, J. Cui, J. Zou, M. Zhu and X. Yao, *Phys. Chem. Chem. Phys.*, 2013, 15, 5814-5820.

26. M. Ismail, Y. Zhao and S. X. Dou, *Int. J. Hydrogen Energy*, 2013, 38, 1478-1483.

27. G. S. Walker, M. Abbas, D. M. Grant and C. Udeh, *Chem. Commun.*, 2011, 47, 8001-8003.

28. M. Ismail, Y. Zhao, X. B. Yu and S. X. Dou, *RSC Advances*, 2011, 1, 408-414.

29. Y. Zhang, Q.-F. Tian, S.-S. Liu and L.-X. Sun, *J. Power Sources*, 2008, 185, 1514-1518.

30. M. Ismail, Y. Zhao, X. B. Yu and S. X. Dou, *Int. J. Hydrogen Energy*, 2012, 37, 8395-8401.

31. R. A. Varin, M. Jang, T. Czujko and Z. S. Wronski, *J. Alloys Comp.*, 2010, 493, L29-L32.

32. H. Shao, M. Felderhoff and F. Schüth, *Int. J. Hydrogen Energy*, 2011, 36, 10828-10833.

33. B. Zhang and Y. Wu, *Int. J. Hydrogen Energy*, 2014, 39, 13603-13608.

34. H. Leng, Y. Pan, Q. Li and K.-C. Chou, *Int. J. Hydrogen Energy*, 2014, 39, 13622-13627.

35. M. Ismail, N. Juahir and N. S. Mustafa, *J. Phys. Chem. C*, 2014, 118, 18878-18883.

36. M. Ismail, Y. Zhao, X. B. Yu and S. X. Dou, *Energy Edu. Sci. Technol. Part A Energy Sci. Res.*, 2012, 30(SPEC .ISS.1), 107-122.

37. X. Xiao, S. Wang, X. Fan, C. Xu, J. Sun, Q. Wang and L. Chen, *Int. J. Hydrogen Energy*, 2014, 39, 6577-6587.

38. D. Kyoi, T. Sakai, N. Kitamura, A. Ueda and S. Tanase, *J. Alloys Comp.*, 2008, 463, 311-316.

39. N. S. Mustafa and M. Ismail, *Int. J. Hydrogen Energy*, 2014, 39, 15563-15569.

40. Z.-Q. Sun, D.-M. Sun, A.-X. Li and Z.-Y. Xu, *Chin. Phys. Lett.*, 1999, 16, 389.

41. Http://www.chemistry-reference.com/StandardThermodynamicValuesat25°C.

42. M. V. Glazoff, *Thermodynamic Assessment of Hot Corrosion Mechanisms of Superalloys Hastelloy N and Haynes 242 in Eutectic Mixture of Molten Salts KF and ZrF_4*, 2012, INL/EXT-12-24617,Revision 0, 4.

43. W. Luo, V. Stavila and L. E. Klebanoff, *Int. J. Hydrogen Energy*, 2012, 37, 6646-6652.

44. J. Wang, T. Liu, G. Wu, W. Li, Y. Liu, C. M. Araújo, R. H. Scheicher, A. Blomqvist, R. Ahuja, Z. Xiong, P. Yang, M. Gao, H. Pan and P. Chen, *Angew. Chem. Int. Ed.*, 2009, 48, 5828-5832.

45. R. A. Jat, S. C. Parida, R. Agarwal and K. L. Ramakumar, *Int. J. Hydrogen Energy*, 2014, 39, 14868-14873.

46. D. Chattaraj, S. C. Parida, S. Dash and C. Majumder, *Int. J. Hydrogen Energy*, 2014, 39, 9681-9689.

Figure captions

Figure 1- TPD patterns for the dehydrogenation of as-received MgH_2, as-milled MgH_2 and the MgH_2 doped with 5 wt.%, 10 wt.%, 15 wt.% and 20 wt.% K_2ZrF_6.

Figure 2- Isothermal absorption kinetics measurement of as-milled MgH_2 and MgH_2 doped with 5 wt.%, 10 wt.%, 15 wt.% and 20 wt.% K_2ZrF_6 at 300 ºC.

Figure 3-Isothermal desorption kinetics curves for as-milled MgH_2 and MgH_2 doped with 5 wt.%, 10 wt.%, 15 wt.% and 20 wt.% K_2ZrF_6 at 300 ºC.

Figure 4- Isothermal dehydrogenation curves of as-milled MgH_2 and 10 wt.% K_2ZrF_6-doped MgH_2 at 300 °C (a, d), 320 °C (b, e) and 350 °C (c, f).

Figure 5- Arrhenius plots of ln(k) vs 1/T for as-milled MgH_2 and MgH_2 + 10wt.% K_2ZrF_6.

Figure 6- Isothermal rehydrogenation kinetics of the MgH_2+10 wt.% K_2ZrF_6 composite in the 1st, 5th and 10th cycles.

Figure 7- Isothermal dehydrogenation kinetics of the MgH_2+10 wt.% K_2ZrF_6 composite in the 1st, 5th and 10th cycles.

Figure 8- SEM image for as-received MgH_2 (a), as-milled MgH_2 (b) and the MgH_2 doped with 10 wt.% K_2ZrF_6 (c).

Figure 9- X-ray diffraction patterns of MgH_2-10 wt.% K_2ZrF_6 (a) after milling, (b) after dehydrogenation, and (c) after rehydrogenation.

Figure 10- X-ray diffraction patterns of MgH_2-20 wt.% K_2ZrF_6 (a) after milling, (b) after dehydrogenation and (c) after rehydrogenation.

Figures

Figure 1

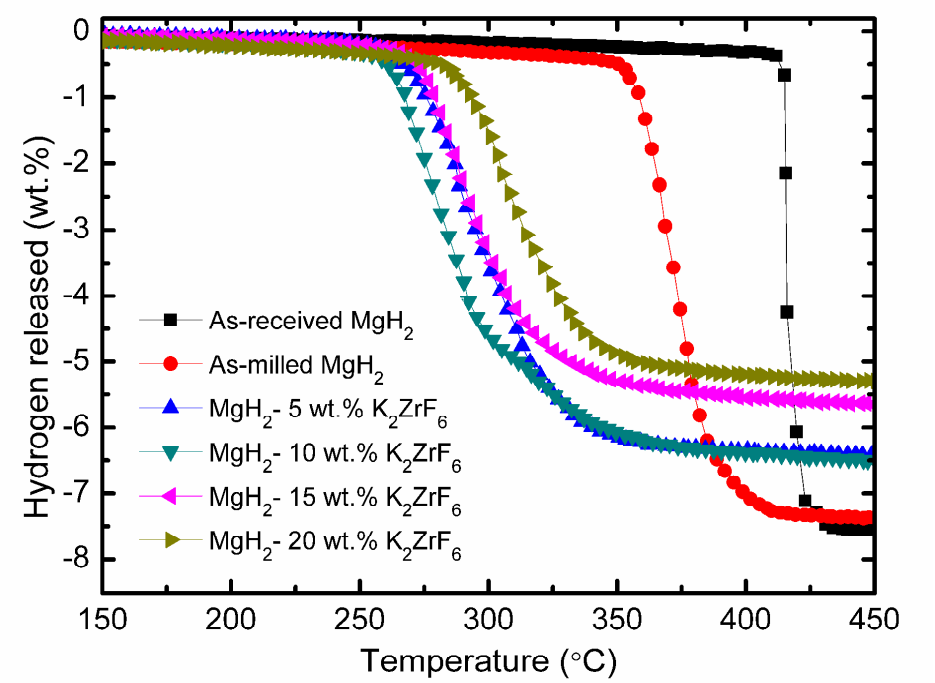

Figure 2

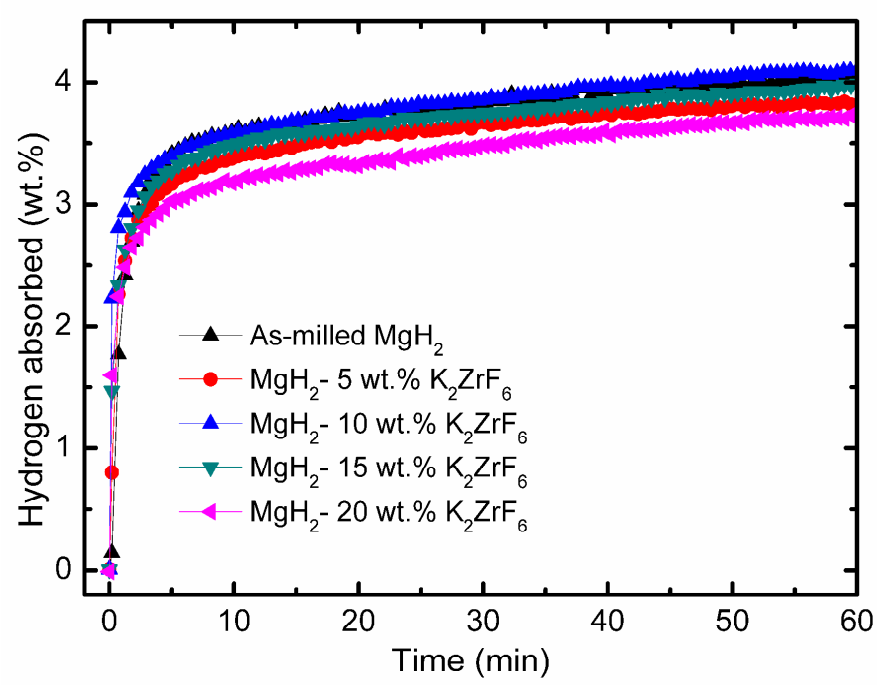

Figure 3

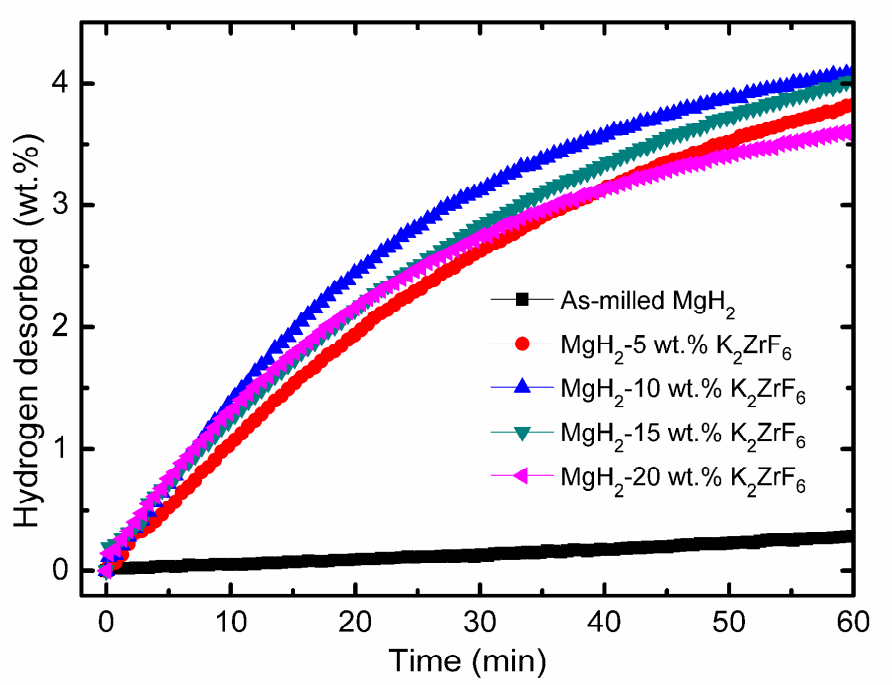

Figure 4

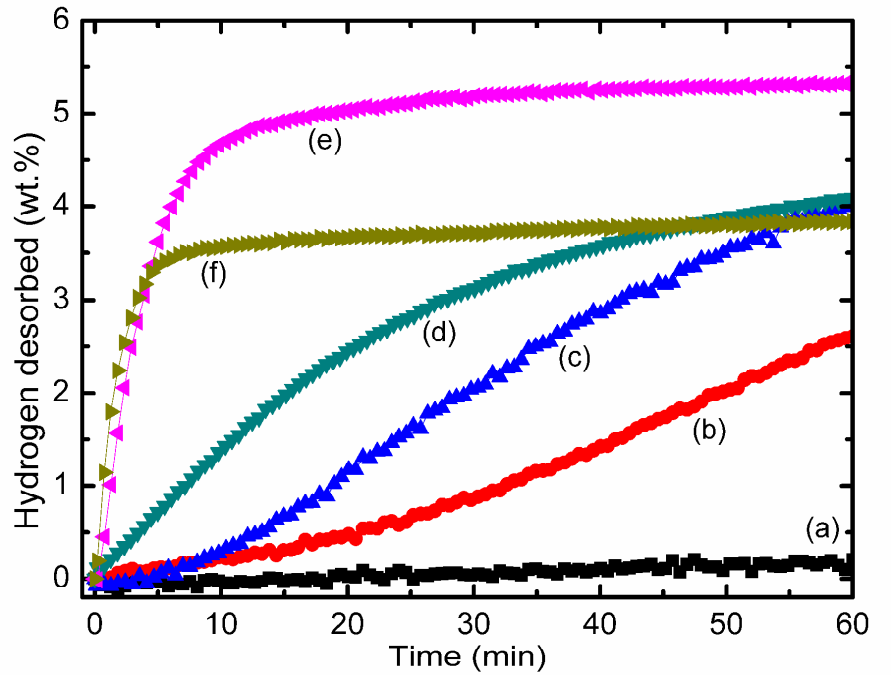

Figure 5

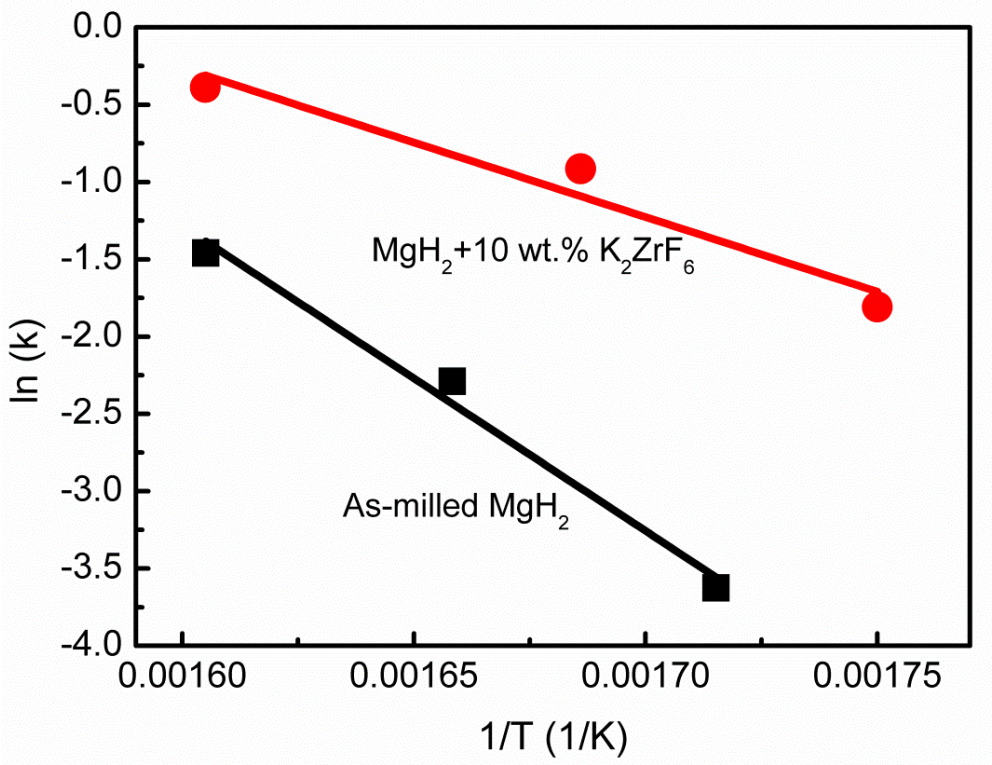

Figure 6

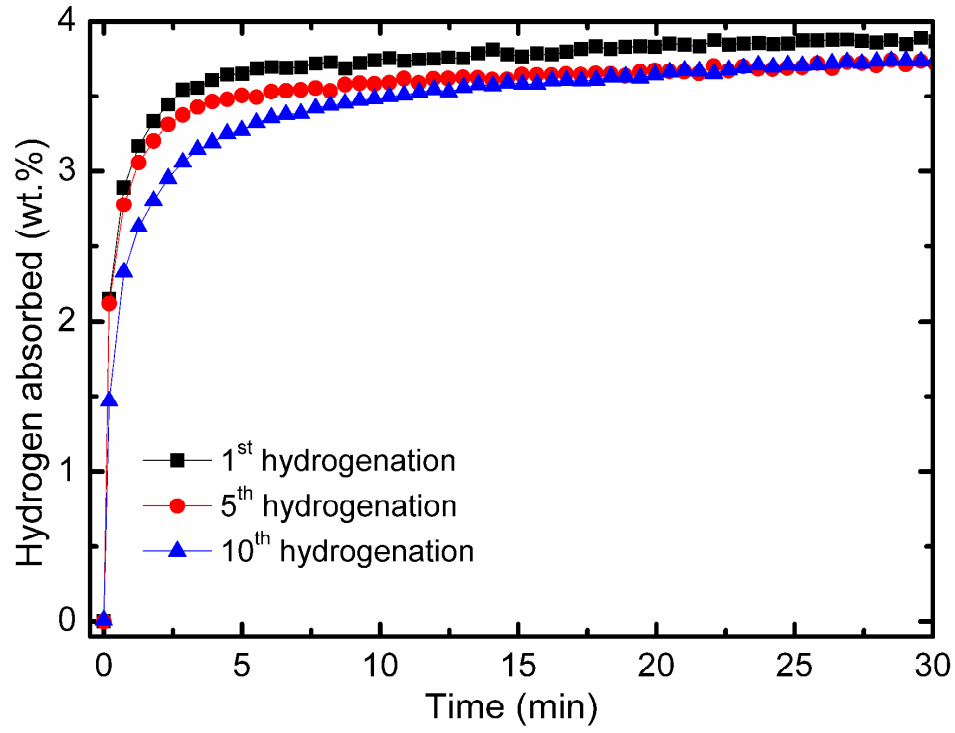

Figure 7

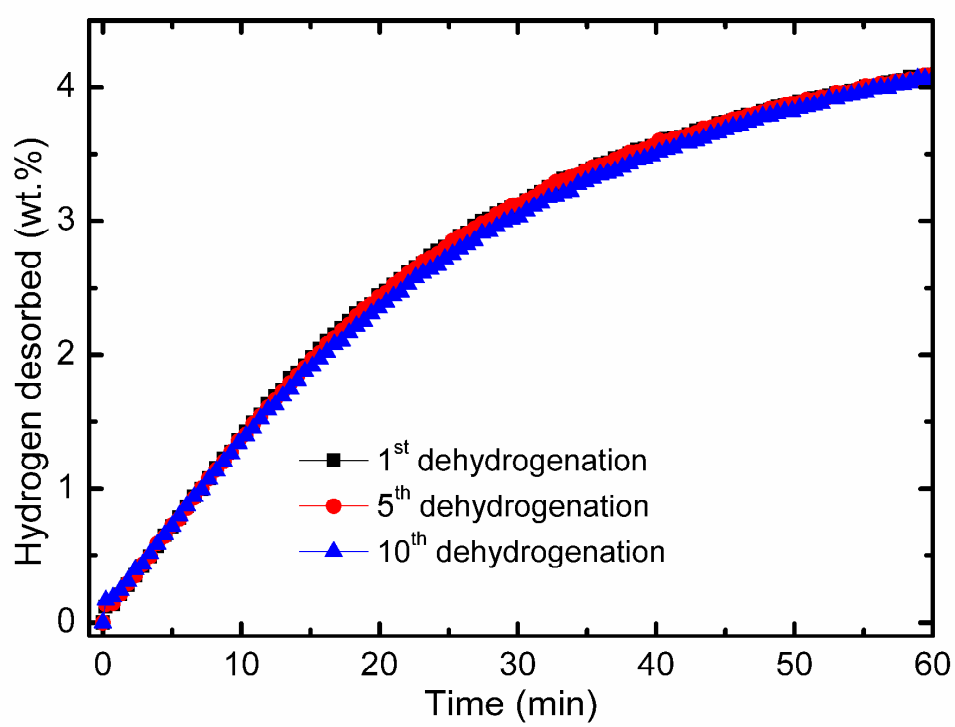

Figure 8

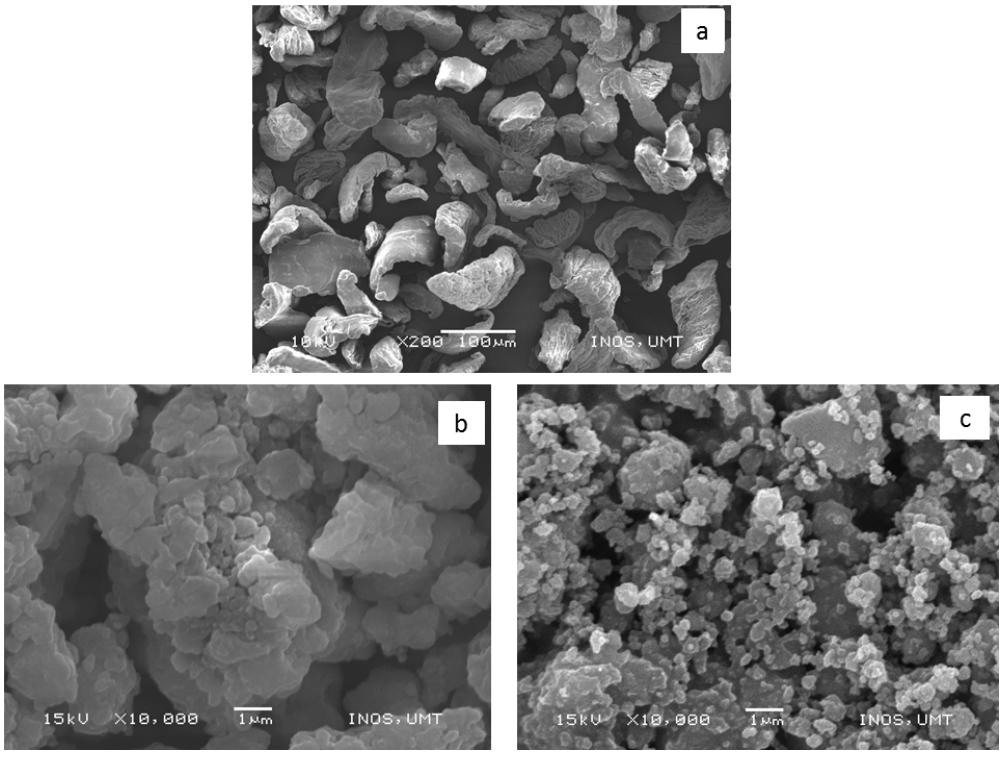

Figure 9

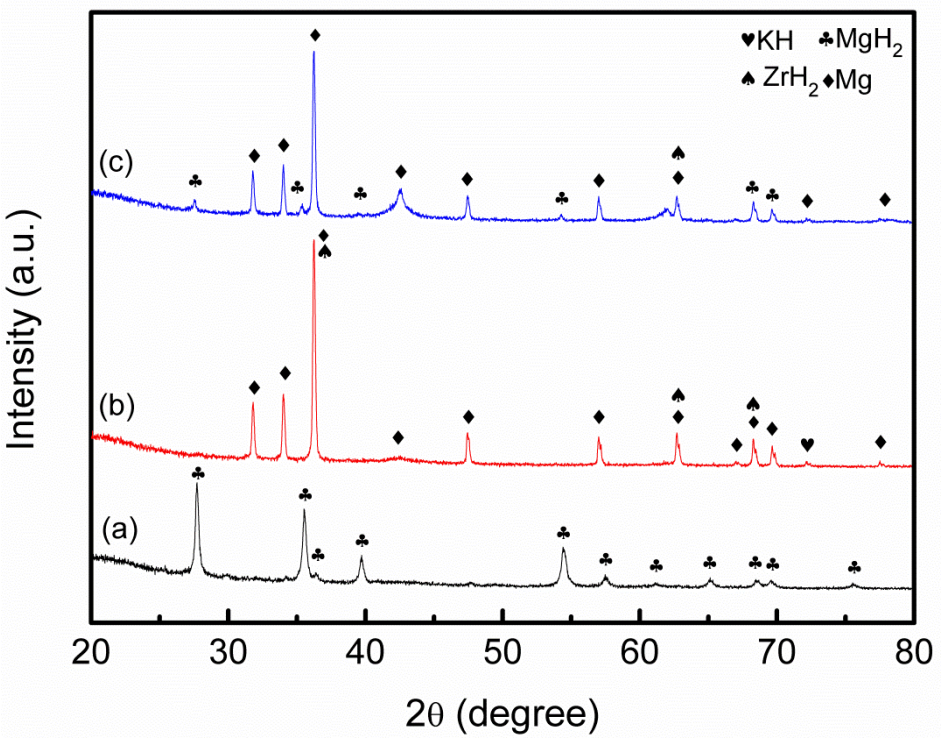

Figure 10